Polyhedron 261 (2024) 117128

Contents lists available at ScienceDirect

Polyhedron

journal homepage: www.elsevier.com/locate/poly

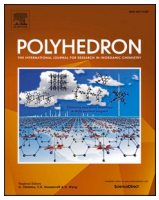

Manganese(III) complexes with a tetradentate thiosemicarbazone. Structural characterization, electrochemistry, antioxidant capability, molecular docking and dynamics simulation on the potential inhibitory activity of cyclin-dependent kinase 2

Sinem Ortaboy [a,*], Tuncay Karakurt [c], Büşra Kaya [b], Onur Şahin [d], Bahri Ülküseven [b]

[a] Physical Chemistry Division, Department of Chemistry, Engineering Faculty, Istanbul University-Cerrahpaşa, 34320, Avcılar, Istanbul, Türkiye
[b] Inorganic Chemistry Division, Department of Chemistry, Engineering Faculty, Istanbul University-Cerrahpaşa, 34320, Avcılar, Istanbul, Türkiye
[c] Department of Chemical and Process Engineering, Faculty of Engineering-Architecture, Ahi Evran University, 40100 Kirsehir, Türkiye
[d] Department of Occupat Health & Safety, Faculty of Health Sciences, Sinop University, Sinop TR-57000, Türkiye

ARTICLE INFO

Keywords:
Manganese
Thiosemicarbazone
Electrochemistry
Antioxidant performance
Molecular docking

ABSTRACT

Two manganese(III) complexes with the general formula $[Mn^{III}(L)X]$ (where L is a tetradentate thiosemicarbazone; X = Cl (Mn1) or N_3 (Mn2 is new) were synthesized and verified the expected structures by experimental and theoretical methods. Electrochemical behavior of the manganese complexes were studied using cyclic voltammetry (CV) and square wave voltammetry (SWV). TEAC and DPPH values were determined and compared with those of ascorbic acid (AA). Further, the correlation between the antioxidant data and redox potentials was discussed. Molecular dynamics (MD) simulations were performed after calculating the binding affinities to cyclin-dependent kinase 2 for Mn1, Mn2, and AA to clarify some information about their thermodynamic and dynamic properties and to validate the molecular docking results. The calculations gave the binding affinities that are −6.0, −8.6 and −9.4 kcal/mol for AA, Mn1 and Mn2, respectively. The experimental and theoretical results revealed that complex Mn2 having azide ion has a better antioxidant performance and also the highest docking score with the protein. The study demonstrated that such manganese complexes are suitable candidates to drug development against diseases caused by oxidative stress.

1. Introduction

Biologically functional metals have always attracted attention, and the compounds containing any of these are significant topics of pro-drug research for diseases caused by bacteria, viruses, or dysregulated cell mechanisms [1–5]. Manganese is involved in vital redox processes including macronutrient metabolism and free radical defense systems. It is a cofactor for many enzymes, such as manganese-superoxide dismutase, an antioxidant enzyme that protects the cell against damage caused by free radicals [6–9]. Considering the relationship between free radicals and many diseases, especially cancer, the importance of examining the redox and antioxidant features of manganese compounds is understood. Therefore, an increasing number of studies have been published on the electrochemistry [10–13] and antioxidant properties [14–17] of manganese compounds.

In electrochemistry studies, cyclic voltammetry (CV) and square wave voltammetry (SWV) techniques are favored to clarify the electrochemical potential, structure and activity relationship of metal complexes because they provide more sensitive, rapid, and accurate results than other techniques. Especially, they are extensively used for analyzing the redox status of metal complexes and the antioxidant content of biological samples [18].

Thiosemicarbazone derivatives are an important class of N, S-donor ligands exhibiting superior coordination tendency, high selectivity, and stability towards a wide variety of metal ions. They can coordinate as neutral (keto form) molecules or, after deprotonation, as anionic (enol form) ligands and can adopt various coordination modes with different metal ions. They exhibit various biological activities such as antitubercular, antimalarial, antibacterial, antiviral, antiproliferative, antioxidant, and antitumor activities and they are studied for their potential applications in medicinal chemistry. The diverse range of biological activities exhibited by thiosemicarbazones makes them interesting

* Corresponding author.
E-mail address: ortaboy@iuc.edu.tr (S. Ortaboy).

https://doi.org/10.1016/j.poly.2024.117128
Received 28 February 2024; Accepted 28 June 2024
Available online 29 June 2024

compounds for further research and development in the field of drug discovery [19].

As a matter of course, researching the metal complexes obtained from biologically active molecules is primarily preferred [20–24]. Thiosemicarbazones have a wide range of biological activity and the electrochemistry of many manganese complexes derived from tridentate derivatives has been studied. There are also a few reports on manganese complexes of tetra [25,26] and pentadentate [27,28] ones.

Here we present the experimental and theoretical studies on tetradentate thiosemicarbazone as well as two manganese(III) complexes bearing chlorine or azide ions as co-ligands (Fig. 1). Antioxidant capacity defined by TEAC coefficient, DPPH value, and free radical scavenging activity was determined and evaluated correlation with the redox potentials obtained from cyclic and square wave voltammetry experiments. To predict the behavior of the manganese complexes in biological environments, the quantum chemical activation and molecular dynamic simulation data giving an idea about interaction probabilities with proteins were calculated. Ascorbic acid (AA) was a comparison item in all experiments.

2. Experimental

2.1. Synthesis

Acetylacetone-S-methylthiosemicarbazone hydrogen iodide (TSC) was prepared according to the literature method [29]. The manganese complexes with tetradentate thiosemicarbazone ligand were prepared from the template condensation of TSC and salicylaldehyde in the presence of $MnCl_2$ [30]. In the reaction mixture, a square pyramid structure, [Mn(L)X)] (X = Cl or N_3), is formed by oxidation of the manganese center from 2 + to 3 + with air. Complex Mn1, which its full characterization was given in the previous study [31], freshly prepared for this study was confirmed by elemental analysis and IR data. The new complex, Mn2, was synthesized by the reaction of the Mn1 with NaN_3 (Fig. 1). To a solution of (0.5 mmol) the complex Mn1 in 10 mL of methanol-dichloromethane (1:1) was added solution of NaN_3 (1.5 mmol) in 10 mL of methanol. The mixture was refluxed for 2 h. The black-looking crystals were filtered off and recrystallized from the methanol-dichloromethane mixture.

Elemental analysis was carried out in a Thermo Finnigan Flash EA 1112 CHNS analyzer, magnetic measurements were performed in an MK I model device from Sherwood Scientific, and obtained infrared spectra in an Agilent Carry 630 FTIR spectrometer. Electrospray ionization mass spectrometry (ESI-MS) data of Mn2 were collected using a Thermo Finnigan LCQ advantage MAX LC/MS/MS in $CHCl_3$.

Mn1, monochloro N1-acetylacetone-N4-salicylidene-S-methylthiosemicarbazidato-manganese(III). Yield: 24 %; m.p. (°C): >350; μeff (BM): 4.82; Anal. Calc. for $C_{14}H_{15}N_3O_2SMnCl$ (379.75 g mol-1): C, 44.28; H, 3.98; N, 11.07; S, 8.44. Found: C, 43.88; H, 3.67; N, 10.73; S, 8.17 %. IR (cm-1): ν(C = N1) 1602; ν(N2 = C) 1567; ν(N4 = C) 1558; ν(C—O) 1140, 1115.

Mn2, *monoazido N^1-acetylacetone-N^4-salicylidene-S-methylthiosemicarbazidato-manganese(III)*. Yield: 18 %; m.p. (°C): >350; μ_{eff} (BM): 4.79; *Anal. Calc.* for $C_{14}H_{15}N_6O_2SMn$ (386.31 g mol^{-1}): C, 43.53; H, 3.91; N, 21.75; S, 8.30. Found: C, 43.39; H, 3.78; N, 21.64; S, 8.04 %. IR (cm^{-1}): ν(C = N^1) 1602; ν(N^2 = C) 1574; ν(N^4 = C) 1558; ν(C—O) 1138, 1121, ν(N_3) 2038. + c ESI MS (*m/z*, relative abundance%): [M−N_3] 344.1 (100 %).

2.2. X-ray crystallography

A suitable crystal of Mn2 was selected for data collection which was performed on a D8-QUEST diffractometer equipped with graphite-monochromatic Mo-K_α radiation at 296 K. The structure was solved by direct methods using SHELXS-2013 [32] and refined by full-matrix least-squares methods on F^2 using SHELXL-2013 [33]. All non-hydrogen atoms were refined with anisotropic parameters. The H atoms were located from different maps and then treated as riding atoms with C—H distances of 0.93–0.96 Å. The following procedures were implemented in our analysis: data collection: Bruker APEX2 [34]; program used for molecular graphics were as follows: MERCURY programs [35]; software used to prepare material for publication: WinGX [36]. Details of data collection and crystal structure determinations were given in Table 1.

2.3. Electrochemistry

All electrochemical measurements were carried out on a Gamry Reference 600 Potentiostat/Galvanostat ZRA system (Gamry Instruments, Inc., Warminster, PA, USA) coupled with a conventional three-electrode design. A bare glassy carbon electrode (GCE, in 3.0 mm diameter) served as the working electrode (WE), while a saturated Ag/AgCl was utilized as the reference electrode (RE), and a platinum wire was used as the counter electrode (CE). To prevent Ag^+ and Cl^- ions from leaking into the WE compartment double bridged design was adopted for RE. All data were recorded and processed with an Echem Analyst Software interfaced with a PC. Electrochemical experiments

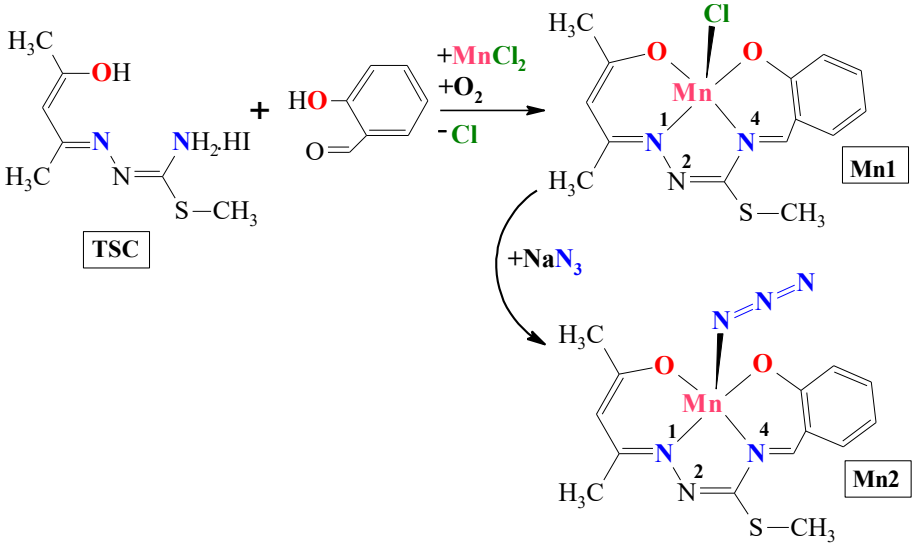

Fig. 1. Synthesis scheme of the manganese(III)-thiosemicarbazone complexes.

Table 1
Crystal data and structure refinement parameters for Mn2.

Empirical formula	$C_{14}H_{15}MnN_6O_2S$
Formula weight	386.32
Crystal system	Triclinic
Space group	*P*-1
a (Å)	7.6889 (11)
b (Å)	8.8676 (16)
c (Å)	13.528 (2)
α (°)	96.221 (9)
β (°)	99.649 (8)
γ (°)	109.165 (8)
V (Å^3)	845.6 (2)
Z	2
D_c (g cm^{-3})	1.517
μ (mm^{-1})	0.92
Measured refls.	20,538
Independent refls.	3220
R_{int}	0.056
S	1.01
R1/w*R*2	0.068/0.164
$\Delta\rho_{max}/\Delta\rho_{min}$ (eÅ^{-3})	0.41/-0.42
CCDC	2,223,611

were conducted in dimethylsulfoxide (DMSO) or dichloromethane (DCM) containing 0.1 M tetrabutylammonium perchlorate (TBAP) as the supporting electrolyte. Unless otherwise specified, 0.1 mM Mn1 and Mn2 analyte concentrations were used in the experiments. Before each run, high-purity nitrogen (N_2) was purged through the supporting electrolyte to remove all dissolved oxygen for 10 min. A nitrogen atmosphere was maintained over the cell during measurements. All experiments were performed at room temperature (25 °C) and atmospheric pressure. During experiments, the uncompensated resistance between the WE and RE was corrected using IR compensation mode. Before each set of experiments, GCE was polished with 1.00 and 0.05 μm alumina powder, respectively, and rinsed thoroughly with deionized (DI) water between each polishing step. Then it was sonicated successively in ethyl alcohol and DI water for 15 min. Finally, the cleaned electrode was dried with a high-purity N_2 steam.

2.4. Antioxidant tests

TEAC values of the complexes were obtained by the CUPRAC method [37]. The method is based on the absorbance measurement of Cu(I)-neocuproine (Nc) chelate formed as a result of the redox reaction of antioxidants with Cu(II)–Nc. To a test tube were added 1 mL of 10 mM $CuCl_2{\cdot}2H_2O$, 1 mL of 7.5 mM Nc, 1 mL of 1.0 M pH 7 NH_4Ac buffer solution, x mL antioxidant sample solution, and (1.1-x) mL H_2O, in this order. The mixture, in a total volume of 4.1 mL, was incubated for 30 min and the absorbance was recorded at 450 nm. The TEAC coefficients (trolox equivalent antioxidant capacities) were calculated as the ratio of the molar absorptivity of each compound to that from the trolox method (ε_{trolox}: 1.67x10^4 L mol^{-1} cm^{-1}).

The radical scavenging activity of the compounds was tested with reference to the DPPH (2,2-diphenyl-1-picrylhydrazyl) radicals [38]. The activities of the compounds were tested at different concentrations (5, 10, 15 and 20 μM). An appropriate volume of the compound solution was mixed with 2 ml of (100 μM) DPPH solution, and it made up to a final volume of 4 ml using methanol. After gently mixing, the solution was incubated in the dark for 30 min and the absorbance was measured at 515 nm. Scavenging activity was calculated by the following equation:

DPPH radical scavenging activity (%) = $[(A_{control} - A_{sample})/A_{control}] \times 100$.

The scavenging percentages were plotted against the different concentrations, and IC_{50} values were calculated from the graph. Since ascorbic acid (AA) was used to compare the antioxidant performances of manganese complexes, the methods were also applied to AA.

3. Results and discussion

3.1. Chemistry

The template condensation of S-methyl derivative (TSC) and salicylaldehyde inducated by manganese ion yields the manganese complexes bearing dibasic N1-acetylacetone-N4-salicylidene-S-methylthiosemicarbazidato ligand [31]. Complex Mn1 was newly prepared and from its reaction with NaN_3, new Mn2 complex with the composition [Mn^{III}(L)N_3] was synthesized (Fig. 1). Thus, an azide ion was attached to the 5th coordination site of manganese (III) instead of the chlorine atom. Mn2 is a stable solid in air such as Mn1 and soluble in DMF, DMSO, alcohols, and chlorinated hydrocarbons. The measured magnetic moment (4.79 BM) for Mn2 is close to that of Mn1 (4.82 BM), and the values point to the 4-electron high-spin state of the manganese(III) ions [39].

The template reaction involves two simultaneous steps which are ligand formation by amine-aldehyde condensation and its binding to the metal ion. Complex formation can be monitored by infrared spectra (**Fig. S1**). The amine and hydroxyl bands of TSC were absent in the spectrum of Mn2 due to the condensation of the NH_2 and deprotonation of the OH. Azomethine (C═N) and azide (N_3) bands of Mn2 were recorded at 1602, 1558, and 2038 cm^{-1}, respectively. In the ESI mass spectrum of Mn2, the expected molecular mass peak [M] was recorded at *m/z* 386.8 at the lowest intensity (relative abundance < 5 %). The most prominent peak was observed at *m/z* 344.1, corresponding to [M−N_3] (**Fig. S2**).

3.2. Crystallography

The molecular structure of complex Mn2, with the atom numbering scheme, is shown in Fig. 2. The asymmetric unit of Mn2 contains one manganese ion, one thiosemicarbazone ligand, and one azide ion. The manganese (III) ion is coordinated by two oxygen atoms [Mn1-O1 = 1.881(4) Å and Mn1-O2 = 1.890(4) Å] and two nitrogen atoms [Mn1-N1 = 1.980(4) Å and Mn1-N3 = 1.951(5) Å] from the ligand and a nitrogen atom of azide group [Mn1-N4 = 2.095(5) Å]. The coordination geometry around the manganese center is a slightly distorted square pyramid using the O1-Mn1-N3 and O2-Mn1-N3 angle values given in Table 2, the Addison tau parameter (τ) was calculated as 0.033. This value close to zero indicates that the distortion is at a very low level. The molecules of Mn2 are connected by C—H•••O and C—H•••N hydrogen bonds (Table 2-Table 3). Chlorine atom (C12) in the molecule at (x, y, z) acts as a hydrogen-bond donor to N6^{ii} atom, so forming a centrosymmetric $R_2^2(16)$ ring centered at (1/2, 1/2, 1). Atom C9 in the molecule at (x, y, z) acts as a hydrogen-bond donor to O1^{i} atom, so forming a C(7) chain which is running parallel to the [1 1 0] direction. The combination of these hydrogen bonds produces edge-fused $R_2^2(16)R_4^4(28)$ rings (Fig. S3). Similarly, C14 in the molecule at (x, y, z) acts as a hydrogen-bond donor to N6^{iii} atom, so forming a C(8) chain which is running parallel to the [1 0 0] direction (Fig. S4).

3.3. Electrochemistry

The voltammetric behavior of Mn1 and Mn2 complexes was investigated by CV and SWV techniques to clarify their redox activities. Electrochemical redox potentials of Mn1 and Mn2 were obtained from both CV and corresponding SW voltammograms. The solvent effect on the electrochemical behavior of Mn1 and Mn2 complexes were investigated using DMSO and DCM as supporting electrolyte containing 0.1 M Tetrabutylammonium perchlorate (TBAP).

As shown in Fig. 3 and Fig. S5, complex Mn1 gave metal-based oxidation for Mn^{II}/Mn^{III} and Mn^{III}/Mn^{IV} at around 0.03 V and 0.76 V, respectively, at relatively low scan rates (Fig. 3 inset). The corresponding reduction peak of Mn^{III}/Mn^{II} was observed at around 0.15 V while that of Mn^{III}/Mn^{IV} was not observed on the return scan, showing

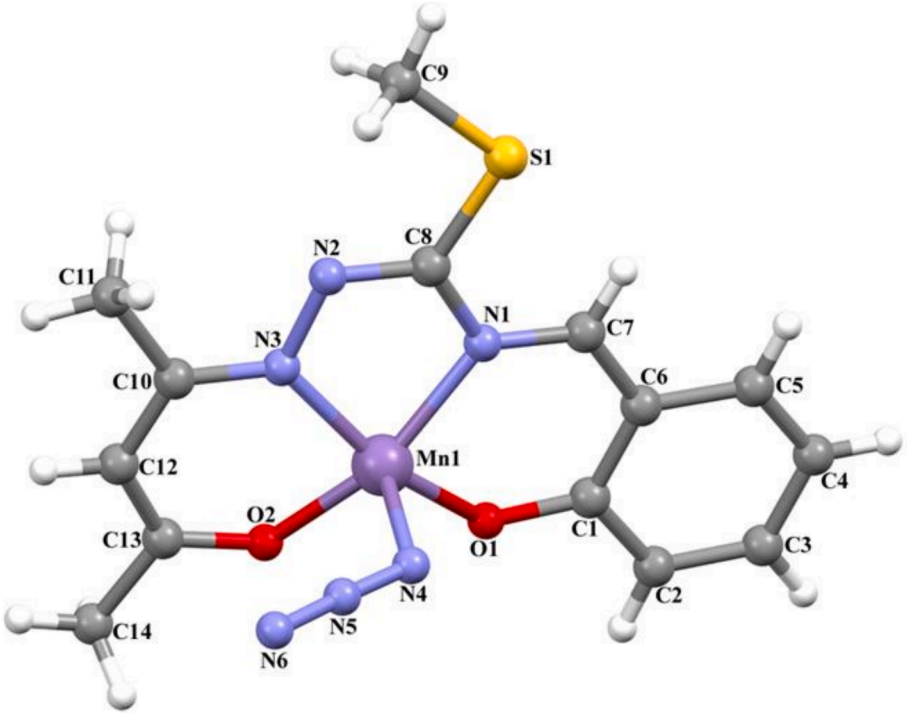

Fig. 2. The molecular structure of Mn2 showing the atom numbering scheme.

Table 2
Selected bond distances and angles for complex Mn2 (Å, °).

Mn1-O1	1.881(4)	Mn1-O2	1.890(4)
Mn1-N3	1.951(5)	Mn1-N1	1.980(4)
Mn1-N4	2.095(5)		
O1-Mn1-O2	93.55(18)	O1-Mn1-N3	162.3(2)
O2-Mn1-N3	91.23(19)	O1-Mn1-N1	90.56(18)
O2-Mn1-N1	160.32(19)	N3-Mn1-N1	79.51(19)
O1-Mn1-N4	101.2(2)	O2-Mn1-N4	99.6(2)
N3-Mn1-N4	94.8(2)	N1-Mn1-N4	98.5(2)

Table 3
Hydrogen-bond parameters for Mn2 (Å, °).

D-H· · ·A	D-H	H···A	D···A	D-H···A
C9—H9B···O1^{i}	0.96	2.58	3.461 (8)	152
C12—H12···N6^{ii}	0.93	2.56	3.451 (11)	161
C14—H14A···N6^{iii}	0.96	2.51	3.427 (12)	161

Symmetry codes: (i) x + 1, y + 1, z; (ii) − x + 1, −y + 1, −z + 2; (iii) x − 1, y, z.

irreversible character. The increase in the scan rates caused the anodic peak potentials to shift in the forward direction at fast scan rates indicating the behavior of the heterogeneous kinetic controlled process on the electrode–electrolyte interface. In addition to the metal-based electron transfer reactions, a ligand-based irreversible oxidation reaction was observed at around 1.42 V.

As mentioned above, CV responses obtained at low scan rates such as 25 mVs^{-1} and 50 mVs^{-1}, show additional redox processes for Mn1 complex (Fig. 3 inset and Fig. S5). These peaks observed at around −0.33 V for reduction and −0.56 V for oxidation processes assigned to the exchange of Cl^{-} ions in Mn1 complex with ClO_4^{-} ions contained in the supporting electrolyte [26].

On the other hand, a significant peak was observed at −1.15 V when 25 Hz frequency was applied. Especially, when the vertex potential reached the ligand-based reduction, the formation of superoxide became prominent which is probably came from the trace amount of water in DMSO. It is well documented that the water moiety is strongly H-bonded to the S═O group in DMSO [41,42]. This reduction peak has an irreversible nature especially at high scan rates since there is no corresponding oxidation peak observed on the CV voltammograms.

Fig. S6 shows the CV curves of complex Mn1 obtained at different potential windows at 100 mVs^{-1} scan rate. From the figure, it revealed that the potential window becomes effective on peak currents and redox processes. The peak currents are relatively small when the CV measurement was recorded in the positive potential region. If the ligand oxidation reaction at 1.46 V was not scanned, the prominent reduction peak of the superoxide species at −1.15 V was almost not observed. This phenomenon indicates that the reduction process of superoxide was initiated by the oxidized form of ligand and electrolysis products originating from trace water in DMSO [43]. Furthermore, it can be seen that when superoxide formation is not observed, ligand reduction peak was detected around −1.42 V as shown in Fig. S6.

For Mn1 in 0.1 M TBAP/DCM medium, two metal-based and two ligand-based redox processes were observed (Fig. 4, and Fig. S7). Formal potentials of metal-based irreversible oxidation process of Mn1 in DCM were recorded at around −0.03 V and 0.52 V for Mn^{II}/Mn^{III} and Mn^{III}/Mn^{IV}, respectively. Those metal centered oxidation peaks became broader as a function of increasing scan rates indicating to the slower charge propagation [44]. Furthermore, ligand-based quasi-reversible oxidation process was effective at around 1.28 V. It was revealed that the ligand-based reduction peak of Mn1 complex shifts to the less negative potential (at around −1.15 V) compared to those of DMSO, which shows the easy electron-accepting behavior of the Mn1 complex in DCM. The difference observed in ligand-based reduction peaks for DCM and DMSO media was attributed to the polarity of DMSO that can be coordinated with the central metal ion [40].

The CV profile of Mn2 showed two metal-based and a ligand-based redox processes at low scan rates in the presence of 0.1 M TBAP/DMSO system (Fig. 5). At relatively low scan rates, two irreversible oxidation processes can be determined at around 0.02 V and 0.60 V related to MnII/MnIII and MnIII/MnIV couples, respectively, and with increasing scan rates the oxidation peak of MnIII/MnIV disappeared. It was mainly attributed to the redox reaction time being slower than the

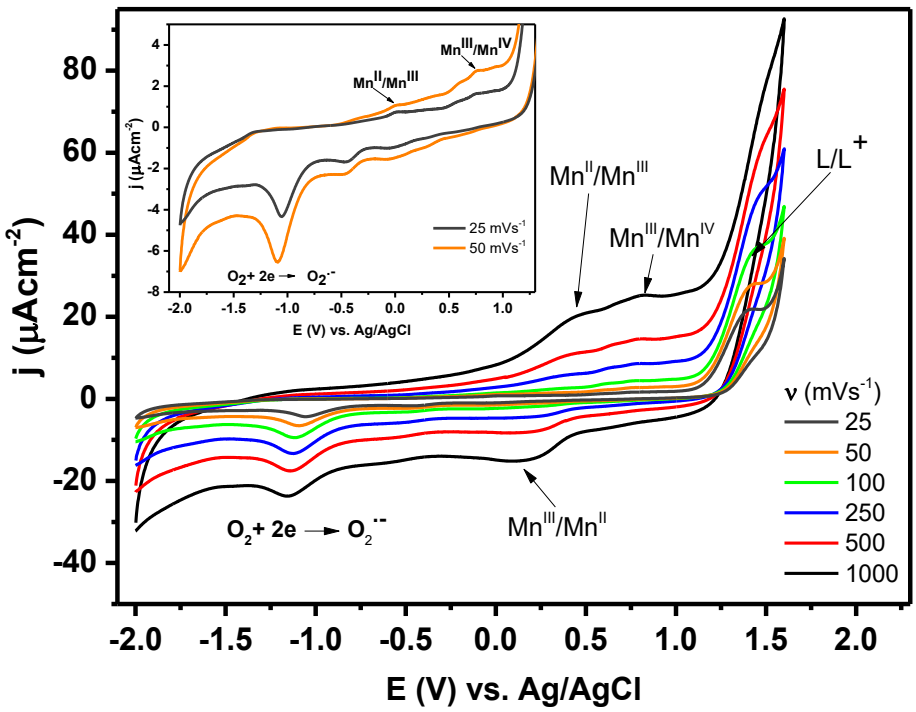

Fig. 3. CV responses of Mn1 complex at various scan rates on a GCE in 0.1 M DMSO/TBAP supporting electrolyte. Inset: CV responses of Mn1 complex at low scan rates on a GCE in 0.1 M DMSO/TBAP supporting electrolyte.

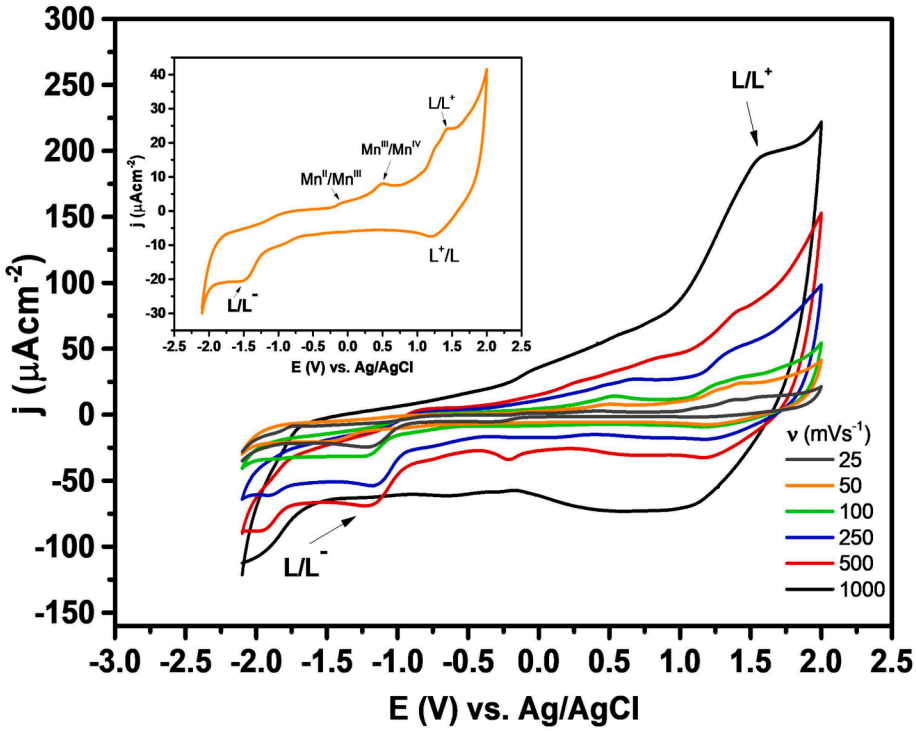

Fig. 4. CV responses of Mn1 complex as a function of increasing scan rates on a GCE in 0.1 M DCM/TBAP supporting electrolyte. Inset: CV responses of Mn1 complex at scan rates of 50 mV/s on a GCE in 0.1 M DCM/TBAP.

fast scan rate. Compared to the complex Mn1 in the same media, the peak potentials of Mn2 slightly shifted to less positive values, indicating a higher antioxidant capacity. The ligand-based reduction process occurs in two steps that their corresponding peaks were located at around −1.56 V and −1.84 V (Fig. 5 and Fig. S8). Similar to this result, in their study on manganese(III)-thiosemicarbazone complex, B. Kaya et al. (2019) reported that two reduction peaks were observed in DMSO while one reduction process was detected for DCM medium [26].

At this stage, we can propose two different models for the charge carrier. The first model could be linked directly to the reduction of N_2 nitrogen of the thiosemicarbazone [45]. It is important to note that the reduction potential of the ligand has split into two distinct peaks, which

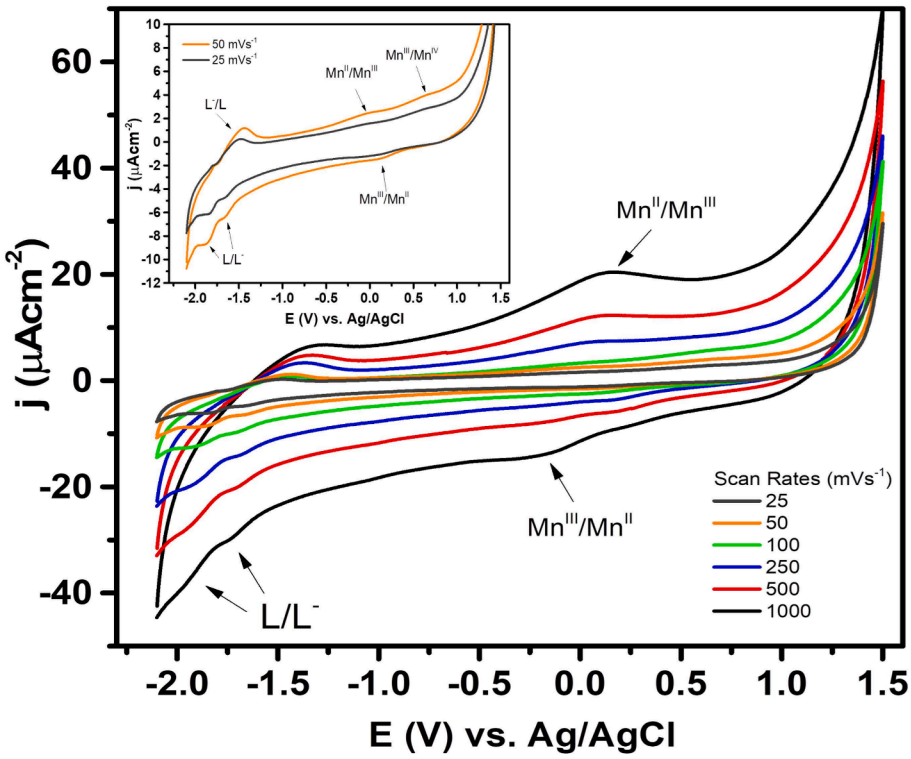

Fig. 5. CV responses of Mn2 complex at various scan rates on a GCE in 0.1 M TBAP /DMSO supporting electrolyte.

is different from complex Mn1 in a TBAP/DMSO environment. The formation of these two peaks implies that the reduction is a result of the interaction between the azide group and DMSO. Alternatively, the second approach could be associated with the reduction of N_3 to form nitrogen containing products such as N_2H_4, N_2, or possibly NH_3, as reported previously [46].

Regarding complex Mn2 in the 0.1 M TBAP/DCM electrolyte, a prominent reduction peak and its shoulder were observed at around −1.02 V and −0.77 V, respectively, at relatively low scan rates (Fig. 6 inset). With increasing scan rate, the shoulder disappeared and the peak potential shifted to more negative potential region. The corresponding oxidation peak was observed at around −0.8 V when applied higher scan rates than 100 mVs^{-1}. In the SW voltammogram (Fig. S9), this peak exhibited a quasi reversible character located at around −0.96 V and

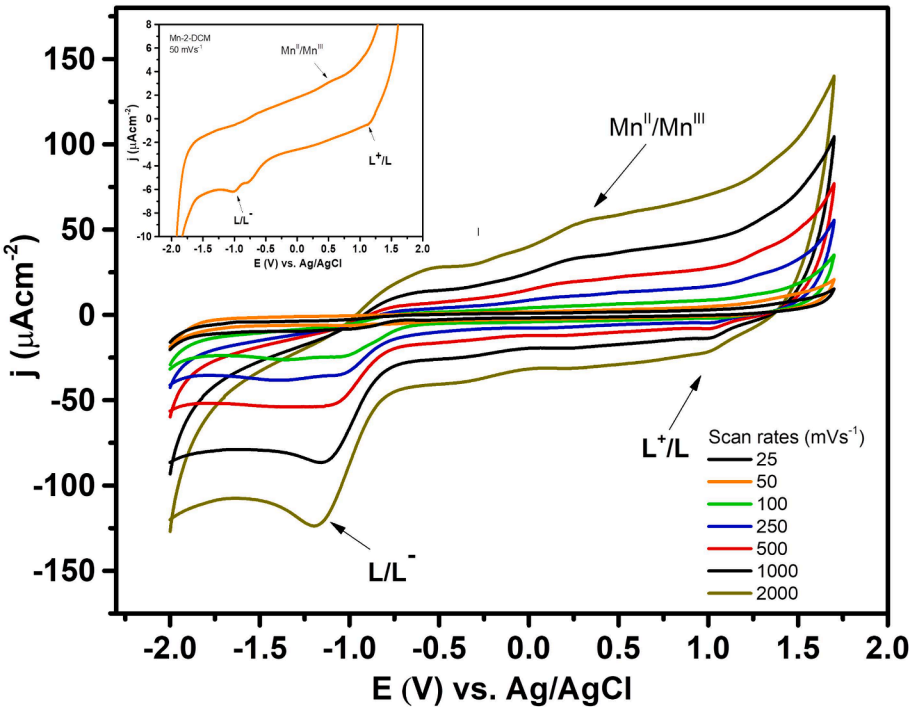

Fig. 6. CV responses of Mn2 complex at various scan rates on a GCE in 0.1 M DCM/TBAP supporting electrolyte.

−0,71 V, respectively, for reduction and oxidation processes. When compared to Mn2 reductions in different media, it was observed that these two reduction peaks slightly shift to the less negative potentials in DCM environment. The polarity of the medium can strongly affect the electrochemical behavior of test molecules [40] and even it is well known that the standard reduction potential of azide/azidyl redox couple decreases from polar to less polar solvents [47,48]. This outcome is might be linked to the increased rate of heterogeneous electron transfer on the electrode/electrolyte interface of azide/azidyl moiety. Relatively ill-defined ligand-based oxidation and reduction processes observed at −1.68 V and −1.62 V respectively, were in agreement with previously reported studies [40,45].

3.4. Antioxidant performance

For evaluate to antioxidant capacities of the manganese(III) complexes, the CUPRAC method was applied. The linear calibration equations of the compounds gave the molar absorption coefficient (ε) as the slope. TEAC (trolox equivalent antioxidant capacities) coefficients, found as the ratio of the molar absorptivity of each compound to that of trolox. The TEAC values were found as follows: Mn2 > Mn1 > AA (see Table 4). The results showed that the manganese(III) complexes were superior to standard AA, especially the TEAC value of Mn2 was found to be approximately three times higher than that of AA.

DPPH free radical scavenging activity is important in determining the ability of an antioxidant agent [49]. DPPH radical scavenging percentage of the manganese(III) complexes and standard AA at different concentrations and their corresponding IC_{50} values were given in Fig. 7 and Table 4, respectively. The DPPH free radical was significantly scavenged by manganese(III) complexes, and the in vitro activity order was compatible with the TEAC values.

The antioxidant activity of manganese(III) complexes of various ligands is frequently investigated to create biomimetic models [50,51]. Schiff-based manganese(III) complexes exhibit significant radical scavenging activity against DPPH, comparable to standard materials [52,53]. In the study where the radical scavenging activity of zinc, manganese, iron, cobalt and nickel complexes with 2,2′-dipicolylamine ligand was measured using the DPPH test and linoleic acid peroxidation, high activity was found for manganese complexes in both tests [54].

The superior antioxidant performance might be due to the nature of the manganese atom. In a study, five manganese(II) complexes were tested for their activity to scavenge the DPPH, ABTS, and hydroxyl radicals and found to be more active than the free ligands [17]. In another study, the antioxidant activities of the Schiff base ligand and its manganese(III) complex were determined by superoxide and hydroxyl radical scavenging methods, and the complex exhibited better performance than its ligand [55].

The fact that complex Mn2 outperformed Mn1 in both tests is probably due to the presence of the azide group. It was reported that in a series of copper(II) complexes of chromone thiosemicarbazone ligands, the electron-donating group at terminal nitrogen enhanced the antioxidant activity, whereas the electron-withdrawing substituent reduced the antioxidant activity [56]. Our previous study revealed that a cobalt (III) complex bearing two azide molecules performed better antioxidant activity than the cobalt(II) complex with the same thiosemicarbazone ligand but without the azide group [57]. Considering the literature data, the relatively high antioxidant performance found for Mn2 and so the positive contribution of electron-rich structures such as azide have been verified.

Table 4
The TEAC coefficients and DPPH results.

	TEAC	DPPH IC_{50} (μM)
Mn1	2.20 ± 0.08	17.9
Mn2	2.84 ± 0.21	12.3
AA	1.02 ± 0.01	8.8

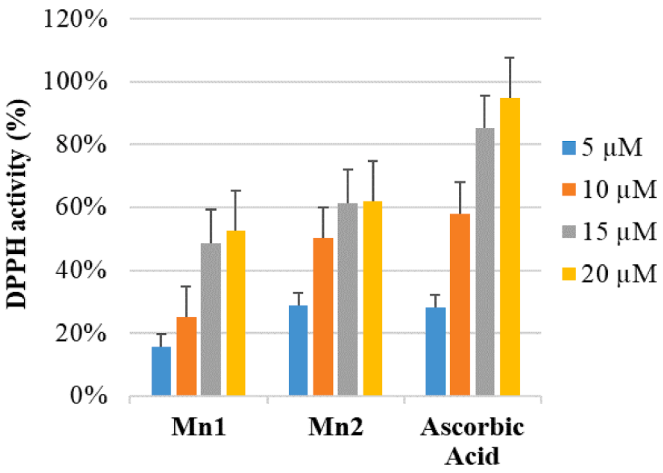

Fig. 7. The free radical scavenging activity of the compounds (%).

Moreover, it is well documented that the higher oxidation potentials lead to lower antioxidant activity due to the more difficult electron transfer kinetics [58]. When considered from this aspect, the antioxidant activity results are also corroborated by the redox data.

3.5. Quantum chemical activate indicatives and molecular docking

Optimizing processes of Mn1, Mn2, and AA molecules and calculations of some parameters were obtained by using the Gaussian 09 program [59] and the DFT/B3LYP/LANL2DZ method [60–62]. The results were visualized using the GaussView 5 program [63] and shown in Fig S9. To shed light on the simulation studies, the molecular electrostatic potential (MEP) surfaces of the optimized compounds were obtained and the nucleophilic and electrophilic regions were determined.

MEP surface map can provide important information about the ligand molecule (herein ligands are Mn1, Mn2, and AA) to be used in drug design [64]. Looking at the MEP surface maps of the molecules (Fig. 8), the red color represents the partially negative charge or electron-rich regions and the blue color partially positive charge or electron-poor regions. In Fig. 8, it was seen that the negative regions were mostly on the O atoms in all three molecules, and the positive regions were on the H atoms in the O—H groups in the AA molecule and on the C—H groups in complexes Mn1 and Mn2.

Molecular Dynamics Simulation (MDS) was performed to study the inhibitory activity of the test compounds for the 4LYN receptor target.

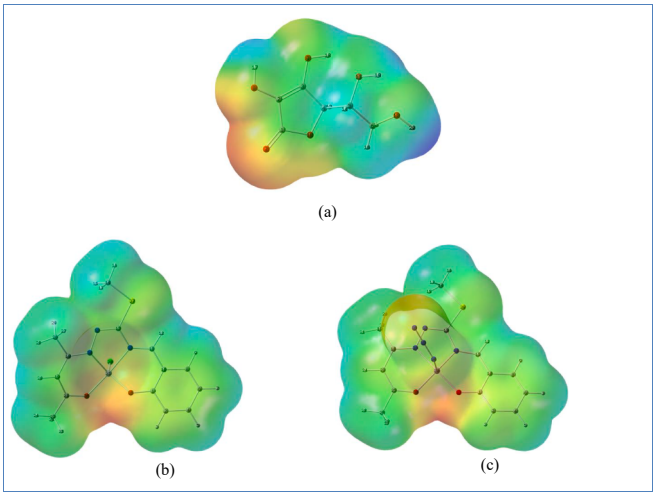

Fig. 8. MEP maps of (a) AA (b) Mn1 (c) Mn2.

Cyclin-dependent kinases (CDKs) are an important group of enzymes in the cell cycle, belonging to the serine/threonine protein kinase group [65]. In cancer cells, CDK regulation is seen in problems with altered expression of CDKs and their regulators, resulting in excessive cell division [66,67]. Due to the importance of CDK's regulatory role in the cell cycle and transcription stage, inhibition of CDKs is seen as a different approach to cancer treatment [68,69].

The crystal structure of 4LYN pdb-encoded Cyclin-Dependent Kinase 2 (CDK2) was downloaded from the Protein Data Bank (PDB; www.rcsb.org). The PyRx program was used to prepare ligand and protein for the docking process, and the Autodockvina program [70], which uses dispersion interactions, hydrogen bonds, electrostatic and desolvation components in the PyRx program [71], was used in the docking process. Gromacs program was used for MDS processes. The ligand–protein complexes obtained by molecular docking were visualized with the BIOVA DS Visualizer 2021 (DSV).

The ligands, Mn1, Mn2, and AA, were successfully placed in the active site of the enzyme (Fig. 9a). Nucleotides located in the binding region of the protein are ASP145, ALA144, ALA31, ILE10, LEU134, VAL64 and PHE80. Both Mn1 and Mn2 interacted with the protein's ALA144 and LEU134 nucleotides, while AA interacted with the ASP145 nucleotide and its receptor by hydrogen bonding (Fig. 9b). Mn1 and Mn2 did not form hydrogen bonds, but were in hydrophobic interaction with the receptor. The calculated binding affinities were −6.0 kcal/mol for AA, while −8.6 and −9.4 for Mn1 and Mn2. According to these values, the Mn2 structure had the highest docking score with the protein. In Fig. 9a, it is also seen that the interaction energy of Mn2 is higher in the active pocket of the receptor compared to the color scale.

3.6. Molecular dynamics

Out files formed as a result of docking processes of receptors and the ligands were used as input files of MDS. In MDS calculation, the AMBER ff14SB force [72] field was used for the protein and AM1-BCC ligand charges [73] for Mn1, Mn2, and AA. For the complex structures formed, x = 15 nm, y = 15 nm, and z = 15 nm were defined by a system in the form of a cubic box. TIP3P water model was added to dissolve the box according to periodic boundary conditions, and sodium (Na^+) and chlorine (Cl^-) ions were added to neutralize the system (Fig. S10). Solvation and ion additions of complexes containing protein and ligands and simulation processes were performed by Gromacs software.

Energy minimization of all systems was done with the steepest descent algorithm and was completed in 1000 steps. In Fig. S11, it was seen that the Potential energy value in the three systems became stable by decreasing. The potential energy change of the three simulated systems was calculated and shown in Fig. S12. The potential energy for the system formed with AA fluctuated between −280000 and −450000 $kJmol^{-1}$ and was stable at about −420000 $kJmol^{-1}$. The potential curve of the systems with Mn1 and Mn2 also exhibited a similar trend. The potential energy curves fluctuated from −320000 to −50000 $kJmol^{-1}$ and the energies were stable around −540000 $kJmol^{-1}$.

Periodic boundary conditions were applied in the simulations and the time step was taken as 10000 ps. After the energy minimization of the systems, the NPT option, which kept the pressure and the temperature constant was passed. The pressure of all three systems was kept at 1 bar with the Berendsen barostat and the temperatures of the systems were kept constant at an average of 300 K with the v-rescale thermostat with a time constant of 0.1 ps. The compressibility constant was 4.5×10^{-5} bar^{-1} and the time constant was 2 ps. Initially, the system temperature was kept at a low value such as 1 K, and the target temperature was reached with a heating rate of 0.1 Kps^{-1}. For long-range interactions, the PME (Particle Mesh Ewald) method [74] was used. The cut-off radius was fixed at 1.4 nm for Van der Waals and short-range Coulomb interactions. From the simulation results, it was determined that the complex structures were stable and the RMSD values were within acceptable (<2.0 Å) values (Fig. S13).

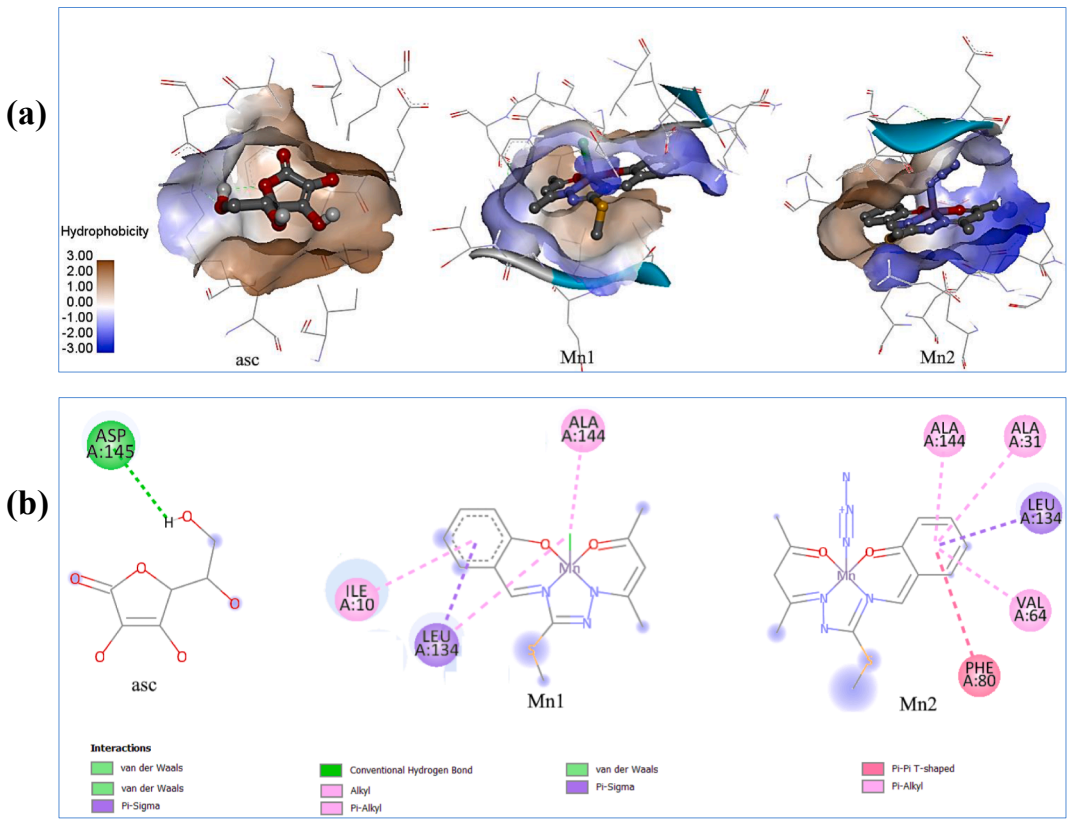

Fig. 9. (a) 3D and (b) 2D Interactions between receptors and ligands.

In Fig. S14, the time-dependent variation of pressure during 10000 ps was shown. According to the pressure–time graph we obtained in the equilibrium step, which lasts for 10000 ps under constant pressure, temperature, and molecular number conditions, these oscillations are around 2 bar, although there are large oscillations in the pressure values during this period. In the density-time graph, the density of the system formed with AA for 10000 ps was observed as an average of 1032 kg m^{-3}, and that of the systems with Mn1 and Mn2 as an average of 1022 kg m^{-3}. These values are very close to the density value of water, 1000 kg m^{-3}. Constant pressure and density values obtained in our pressure–time and density-time graphs showed that our system is in a good equilibrium state.

The interaction energies between the protein and ligands were measured by the short-range (SR) Lennard-Jones (LJ-SR) (Fig. S15a) and Coulomb (Coul-SR) potentials (Fig. S15b). The mean of total interaction energies, Coul-SR and LJ-SR, for the system with AA were calculated as $-$ 150 $\pm$ 28.88 $kJmol^{-1}$, -72 ± 11.73 $kJmol^{-1}$, respectively. These energies were -1176 ± 0.14 $kJmol^{-1}$, -140 ± 11.32 $kJmol^{-1}$ for the system with Mn1 and -159 ± 21.05 $kJmol^{-1}$, -171 ± 11.72 $kJmol^{-1}$ for the system with Mn2. While AA and Mn2 have higher values compared to Mn1 in short-range interaction energies, the system with Mn2 has the highest value in long-range interaction energies.

Hydrogen bond interactions between ligands and protein were unstable according to the interaction distance during 10000 ps and have a continuously increasing character. The average distances of hydrogen bond interactions were 0.13 $\pm$ 0.01 nm, 0.20 $\pm$ 0.01 nm, and 0.19 $\pm$ 0.01 nm for systems including AA, Mn1, and Mn2, respectively (Fig. S16).

4. Conclusion

Two manganese(III) complexes with a tetradentate thiosemicarbazone were synthesized and characterized. Electrochemical behavior and antioxidant performances of the complexes with chlorine or azide as the second ligand were compared by means of experimental findings. To reveal the drug potential, molecular docking, MDS, and RMSD calculations were performed by comparison with ascorbic acid (AA) known antioxidant effect.

In the context of the metal-based oxidations, complex Mn2 has lower oxidation potentials indicating better electron-donating ability than that of the Mn1 complex. This difference is consistent with the TEAC and DPPH data of the complexes and is due to the second ligand azide which is the electron-rich species. Nucleophilic and electrophilic regions that could interact with Cyclin-dependent kinases (CDKs) were identified by MEP maps obtained using the optimized structures of Mn1, Mn2, and AA molecules. The docking of the compounds with the receptor took place through these molecule regions. MDS processes were performed using the complex structures obtained by molecular docking calculations. RMSD values of the three complex systems reached stable values at the end of 180 ps for AA, 28 ps for Mn1, and 1840 ps for Mn2, and RMSD graphs were also quite stable. As a result of the simulation of the receptor-ligands initiated after the docking processes, it was observed that the test molecules bind to the receptor without going too far from the place suggested by the PyRx program.

The data obtained for Mn1 and Mn2 showed that the co-ligand attached to the base structure significantly adjusted the electrochemical and antioxidant properties as well as the quantum mechanical computation results. Considering the experimental and theoretical findings, Schiff base complexes having manganese metal center and azide ion such as Mn2 seem to be suitable agents to be developed for the treatment of diseases caused by oxidative stress.

CRediT authorship contribution statement

Sinem Ortaboy: Writing – original draft, Visualization, Investigation, Formal analysis, Data curation. **Tuncay Karakurt:** Software, Investigation, Formal analysis, Data curation. **Büşra Kaya:** Validation, Investigation, Formal analysis, Data curation. **Onur Şahin:** Investigation, Formal analysis, Data curation. **Bahri Ülküseven:** Writing – review & editing, Writing – original draft, Validation, Supervision, Resources, Methodology, Investigation, Data curation, Conceptualization.

Declaration of competing interest

The authors declare that they have no known competing financial interests or personal relationships that could have appeared to influence the work reported in this paper.

Data availability

Data will be made available on request.

Acknowledgements

The authors acknowledge to Scientific and Technological Research Application and Research Center, Sinop University, Turkey, for the use of the Bruker D8 QUEST diffractometer. Computing resources used in this work were provided by the National Center for High Performance Computing of Turkey (UHeM) under grant number < 1012982022 > . The electrochemical workstation utilized in this work was funded by the Scientific Research Coordination Unit of Istanbul University-Cerrahpaşa with the project numbers FBA-2021-35 414 and FYL-2021-35441.

Appendix A. Supplementary data

Supplementary data to this article can be found online at https://doi.org/10.1016/j.poly.2024.117128.

References

[1] D.E. Reichert, J.S. Lewis, C.J. Anderson, Metal complexes as diagnostic tools, Coord. Chem. Rev. 184 (1999) 3–66, https://doi.org/10.1016/S0010-8545(98)00207-0.
[2] M. Bouché, C. Hognon, S. Grandemange, A. Monari, P.C. Gros, Recent advances in iron-complexes as drug candidates for cancer therapy: reactivity, mechanism of action and metabolites, Dalt. Trans. 49 (2020) 11451–11466, https://doi.org/10.1039/D0DT02135K.
[3] Y. Yu, Q. Xu, S. He, H. Xiong, Q. Zhang, W. Xu, V. Ricotta, L. Bai, Q. Zhang, Z. Yu, J. Ding, H. Xiao, D. Zhou, Recent advances in delivery of photosensitive metal-based drugs, Coord. Chem. Rev. 387 (2019) 154–179, https://doi.org/10.1016/J.CCR.2019.01.020.
[4] A.K. Renfrew, E.S. O'Neill, T.W. Hambley, E.J. New, Harnessing the properties of cobalt coordination complexes for biological application, Coord. Chem. Rev. 375 (2018) 221–233, https://doi.org/10.1016/J.CCR.2017.11.027.
[5] I. Shaikh, I. Shaikh, A. Vohra, R. Devkar, R. Jadeja, Synthesis, characterization, structural features and cytotoxicity of innovative zinc(II) complex derived from ONS-donor thio-Schiff base of acyl pyrazolone, Eur. J. Chem. 10 (2019) 131–138, https://doi.org/10.5155/eurjchem.10.2.131-138.1858.
[6] L.A. Macmillan-Crow, D.L. Cruthirds, Invited review: manganese superoxide dismutase in disease, Free Radic. Res. 34 (2001) 325–336, https://doi.org/10.1080/10715760100300281.
[7] A.K. Holley, V. Bakthavatchalu, J.M. Velez-Roman, D.K. St, Clair, Manganese Superoxide Dismutase: Guardian of the Powerhouse, Int. J. Mol. Sci. 12 (2011) 7114, https://doi.org/10.3390/IJMS12107114.
[8] D.S. Avila, R.L. Puntel, M. Aschner, Manganese in Health and Disease, Met. Ions Life Sci. 13 (2013) 199, https://doi.org/10.1007/978-94-007-7500-8_7.
[9] J. Azadmanesh, G.E.O. Borgstahl, A Review of the Catalytic Mechanism of Human Manganese Superoxide Dismutase, Antioxidants 7 (2018) 25, https://doi.org/10.3390/ANTIOX7020025.
[10] L. Dubois, D.F. Xiang, X.S. Tan, J. Pécaut, P. Jones, S. Baudron, L. Le Pape, J. M. Latour, C. Baffert, S. Chardon-Noblat, M.N. Collomb, A. Deronzier, Binuclear manganese compounds of potential biological significance. 1. Syntheses and structural, magnetic, and electrochemical properties of dimanganese(II) and -(II, III) complexes of a bridging unsymmetrical phenolate ligand, Inorg. Chem. 42 (2003) 750–760, https://doi.org/10.1021/IC020354M.
[11] I. Nar, M. Ozcesmeci, E. Hamuryudan, Synthesis and electrochemical and spectroelectrochemical characterization of chloromanganese(III) phthalocyanines, Turkish J. Chem. 38 (2014) 1064–1072, https://doi.org/10.3906/kim-1405-43.
[12] F.P. Andrew, P.A. Ajibade, Synthesis, Spectroscopic and Electrochemical Study of Mn(II) Complexes of N-methylbenzyl, Phenylpiperazyl- and Morpholinyl-dithiocarbamate, Int. J. Electrochem. Sci. 14 (2019) 7062–7075. https://doi.org/10.20964/2019.08.14.

[13] S. Yadav, S. Kumar, R. Gupta, Manganese Complexes of Pyrrole- and -Indolecarboxamide Ligands: Synthesis, Structure, Electrochemistry, and Applications in Oxidative and Lewis-Acid--Assisted Catalysis, Eur. J. Inorg. Chem. 2015 (2015) 5534–5544, https://doi.org/10.1002/EJIC.201500773.

[14] V.C. Culotta, M.J. Daly, Manganese Complexes: Diverse Metabolic Routes to Oxidative Stress Resistance in Prokaryotes and Yeast, Antioxid. Redox Signal. 19 (2013) 933, https://doi.org/10.1089/ARS.2012.5093.

[15] J.D. Aguirre, V.C. Culotta, Battles with Iron: Manganese in Oxidative Stress Protection, J. Biol. Chem. 287 (2012) 13541, https://doi.org/10.1074/JBC.R111.312181.

[16] G.P. Amaral, G.O. Puntel, C.L. Dalla Corte, F. Dobrachinski, R.P. Barcelos, L.L. Bastos, D.S. Ávila, J.B.T. Rocha, E.O. Da Silva, R.L. Puntel, F.A.A. Soares, The antioxidant properties of different phthalocyanines, Toxicol. In Vitro. 26 (2012) 125–132. https://doi.org/10.1016/J.TIV.2011.10.006.

[17] F. Dimiza, C.P. Raptopoulou, V. Psycharis, A.N. Papadopoulos, G. Psomas, Manganese(II) complexes with the non-steroidal anti-inflammatory drugs naproxen and mefenamic acid: synthesis, structure, antioxidant capacity, and interaction with albumins and DNA, New J. Chem. 42 (2018) 16666–16681, https://doi.org/10.1039/C8NJ03226B.

[18] H.-W. Wang, C. Bringans, A.J.R. Hickey, J.A. Windsor, P.A. Kilmartin, A.R. J. Phillips, Cyclic Voltammetry in Biological Samples: A Systematic Review of Methods and Techniques Applicable to Clinical Settings, Signals 2 (2021) 138–158, https://doi.org/10.3390/SIGNALS2010012.

[19] V. Singh, V.N.V. Palakkeezhillam, V. Manakkadan, P. Rasin, A.K. Valsan, V. S. Kumar, A. Sreekanth, Recent developments on the potential biological applications of transition metal complexes of thiosemicarbazone derivatives, Polyhedron 245 (2023) 116658, https://doi.org/10.1016/j.poly.2023.116658.

[20] B. Ali, M.A. Iqbal, Coordination Complexes of Manganese and Their Biomedical Applications, ChemistrySelect 2 (2017) 1586–1604, https://doi.org/10.1002/SLCT.201601909.

[21] R. Kachadourian, M.M. Flaherty, A.L. Crumbliss, M. Patel, B.J. Day, Synthesis and in vitro antioxidant properties of manganese(III) β-octabromo-meso-tetrakis(4-carboxyphenyl)porphyrin, J. Inorg. Biochem. 95 (2003) 240–248, https://doi.org/10.1016/S0162-0134(03)00135-1.

[22] R.P. John, A. Sreekanth, M.R. Prathapachandra Kurup, H.K. Fun, Chelating behavior of 2-hydroxyacetophenone N(4)-disubstituted thiosemicarbazones: Facile formation of Mn(IV) complexes - X-ray structure, EPR and cyclic voltammetric studies, Polyhedron 24 (2005) 601–610, https://doi.org/10.1016/J.POLY.2005.01.004.

[23] M.K. Bharty, A. Bharti, R. Chaurasia, U.K. Chaudhari, S.K. Kushawaha, P.K. Sonkar, V. Ganesan, R.J. Butcher, Synthesis and characterization of Mn(II) complexes of 4-phenyl(phenyl-acetyl)-3-thiosemicarbazide, 4-amino-5-phenyl-1,2,4-triazole-3-thiolate, and their application towards electrochemical oxygen reduction reaction, Polyhedron 173 (2019) 114125, https://doi.org/10.1016/J.POLY.2019.114125.

[24] R.N. Gautam, A. Tiwari, S. Gupta, M.K. Bharty, V. Ganesan, S. Kumar, P. Bharati, R. J. Butcher, Mn(II) complexes of 1-(4-methoxybenzoyl)-4-phenyl-3-thiosemicarbazide containing o-phenanthroline and 2,2-bipyridine as co-ligands: Synthesis, crystal structure, spectral characterization, photoluminescence and electrochemical studies, J. Mol. Struct. 1278 (2023) 134907, https://doi.org/10.1016/J.MOLSTRUC.2023.134907.

[25] R. Kachadourian, C.A. Johnson, E. Min, I. Spasojevic, B.J. Day, Flavin-dependent antioxidant properties of a new series of meso-N, N′-dialkyl-imidazolium substituted manganese(III) porphyrins, Biochem. Pharmacol. 67 (2004) 77–85, https://doi.org/10.1016/J.BCP.2003.08.036.

[26] B. Kaya, K. Kaya, A. Koca, B. Ülküseven, Thiosemicarbazide-based iron(III) and manganese(III) complexes, Structural, Electrochemical Characterization and Antioxidant Activity, Polyhedron. 173 (2019) 114130, https://doi.org/10.1016/J.POLY.2019.114130.

[27] C. Baffert, M.N. Collomb, A. Deronzier, S. Kjærgaard-Knudsen, J.M. Latour, K. H. Lund, C.J. McKenzie, M. Mortensen, L.P. Nielsen, N. Thorup, Biologically relevant mono- and di-nuclear manganese II/III/IV complexes of mononegative pentadentate ligands, Dalt, Trans. (2003) 1765–1772, https://doi.org/10.1039/B300823A.

[28] S. Krishnan, K. Laly, M.R. Prathapachandra Kurup, Synthesis and spectral investigations of Mn(II) complexes of pentadentate bis(thiosemicarbazones), Spectrochim. Acta Part A Mol. Biomol. Spectrosc. 75 (2010) 585–588, https://doi.org/10.1016/J.SAA.2009.11.022.

[29] C. Yamazaki, The Structure of Isothiosemicarbazones, Can. J. Chem. 53 (1975) 610–615, https://doi.org/10.1139/v75-085.

[30] V.M. Leovac, V.I. Češljević, N.V. Gerbeleu, Y.A. Simonov, A.A. Dvorkin, V.B. Arion, Transition metal complexes with the thiosemicarbazide-based ligands. Part 12. Synthesis, structure and template reaction of ammine [2,4-pentane-dione S-methylisothiosemicarbazonato(2-)] nickel(II) dihydrate, Transit. Met. Chem. 18 (1993) 309–311, https://doi.org/10.1007/BF00207953/METRICS.

[31] B. Kaya, Z.K. Yılmaz, O. Şahin, B. Aslim, Ü. Tükenmez, B. Ülküseven, Structural analysis and biological functionalities of iron(III)– and manganese(III)–thiosemicarbazone complexes: in vitro anti-proliferative activity on human cancer cells, DNA binding and cleavage studies, J. Biol. Inorg. Chem. 24 (2019) 365–376, https://doi.org/10.1007/S00775-019-01653-6.

[32] G.M. Sheldrick, A short history of SHELX, Acta Crystallogr. Sect. A Found. Crystallogr. 64 (2008) 112–122, https://doi.org/10.1107/S0108767307043930.

[33] G.M. Sheldrick, IUCr, SHELXT – Integrated space-group and crystal-structure determination, Urn:Issn:2053-2733. 71 (2015) 3–8. https://doi.org/10.1107/S2053273314026370.

[34] G.M. Sheldrick, APEX2, Bruker AXS Inc., Madison Wisconsin, USA, 2013.

[35] C.F. Macrae, I.J. Bruno, J.A. Chisholm, P.R. Edgington, P. McCabe, E. Pidcock, L. Rodriguez-Monge, R. Taylor, J. Van De Streek, P.A. Wood, Mercury CSD 2.0 – new features for the visualization and investigation of crystal structures, Urn:Issn:0021-8898. 41 (2008) 466–470. https://doi.org/10.1107/S0021889807067908.

[36] L.J. Farrugia, WinGX and ORTEP for Windows: An update, J. Appl. Crystallogr. 45 (2012) 849–854, https://doi.org/10.1107/S0021889812029111.

[37] R. Apak, K. Güçlü, M. Özyürek, S.E. Karademir, Novel Total Antioxidant Capacity Index for Dietary Polyphenols and Vitamins C and E, Using Their Cupric Ion Reducing Capability in the Presence of Neocuproine: CUPRAC Method, J. Agric. Food Chem. 52 (2004) 7970–7981, https://doi.org/10.1021/JF048741X.

[38] C. Sánchez-Moreno, J.A. Larrauri, F. Saura-Calixto, A procedure to measure the antiradical efficiency of polyphenols, J. Sci. Food Agric. (1998), https://doi.org/10.1002/(SICI)1097-0010(199802)76:2.

[39] N. Sarkar, P.K. Bhaumik, S. Chattopadhyay, Manganese(III) complexes with tetradentate salicylaldimine Schiff bases: Synthesis, structure, self assembly and catalase activity, Polyhedron 115 (2016) 37–46, https://doi.org/10.1016/j.poly.2016.04.013.

[40] M. Munakata, S. Kitagawa, M. Miyazima, Classification of Solvents Based on Their Coordination Power to Nickel(II) Ion. A New Measure for Solvent Donor Ability, Inorg. Chem. 24 (1985) 1638–1643, https://doi.org/10.1021/ic00205a009.

[41] H.E. Gottlieb, V. Kotlyar, A. Nudelman, NMR chemical shifts of common laboratory solvents as trace impurities, J. Org. Chem. 62 (1997) 7512–7515, https://doi.org/10.1021/JO971176V.

[42] B. Kirchner, M. Reiher, The secret of dimethyl sulfoxide-water mixtures. A quantum chemical study of 1DMSO-nwater clusters, J. Am. Chem. Soc. 124 (2002) 6206–6215, https://doi.org/10.1021/JA017703G.

[43] M. Hayyan, M.H. Ibrahim, A. Hayyan, M. Ali Hashim, Investigating the long-term stability and kinetics of superoxide ion in dimethyl sulfoxide containing ionic liquids and the application of thiophene destruction, Brazilian, J Chem. Eng. 34 (2017) 227–239, https://doi.org/10.1590/0104-6632.20170341S20150231.

[44] H.M. Naseem Akhtar, A.A. Shaikh, M.Q. Ehsan, Cyclic voltammetric study of the redox behavior of Fe(II)/Fe(III) systems forming during the oxidation of Fe(II) complexes with saccharin and with saccharin and 1,10-phenanthroline, Russian J Elec Chem. 44 (12) (2008) 1403-1408. https://doi.org/10.1134/S102319350812015X.

[45] Y. Kurt, A. Koca, M. Akkurt, B. Ülküseven, Iron(III) and nickel(II) complexes of O, N, N, O-chelating benzophenone thiosemicarbazone: Electrochemistry and in situ spectroelectrochemistry Inorganica Chim, Acta. 388 (2012) 148–156, https://doi.org/10.1016/J.ICA.2012.03.023.

[46] A. Dalmia, S. Wasmus, R.F. Savinell, C.C. Liu, Electrochemical Behavior of Sodium Azide at Pt and Au Electrodes in Sodium Sulfate Electrolyte: A DEMS Study, J. Electrochem. Soc. 142 (1995) 3735–3740, https://doi.org/10.1149/1.2048406/XML.

[47] M.S. Workentin, N.P. Schepp, L.J. Johnston, D.D.M. Wayner, Solvation Control of Chemoselectivity in Reactions of Radical Cations, J. Am. Chem. Soc. 116 (1994) 1141–1142, https://doi.org/10.1021/JA00082A050.

[48] M.S. Workentin, B.D. Wagner, J. Lusztyk, D.D.M. Wayner, Azidyl Radical Reactivity. N6·- as a Kinetic Probe for the Addition Reactions of Azidyl Radicals with Olefins, J. Am. Chem. Soc. 117 (1995) 119–126, https://doi.org/10.1021/JA00106A015.

[49] I. Gülçin, Antioxidant and antiradical activities of l-carnitine, Life Sci. 78 (8) (2006) 803–811, https://doi.org/10.1016/j.lfs.2005.05.103.

[50] G. Lupidi, F. Marchetti, N. Masciocchi, D.L. Reger, S. Tabassum, P. Astolfi, E. Damiani, C. Pettinari, Synthesis, structural and spectroscopic characterization and biomimetic properties of new copper, manganese, zinc complexes: Identification of possible superoxide-dismutase mimics bearing hydroxyl radical generating/scavenging abilities, J. Inorg. Biochem. 104 (2010) 820–830, https://doi.org/10.1016/J.JINORGBIO.2010.03.013.

[51] V. Oliveri, A. Puglisi, G. Vecchio, New conjugates of β-cyclodextrin with manganese(III) salophen and porphyrin complexes as antioxidant systems, Dalt. Trans. 40 (2011) 2913–2919, https://doi.org/10.1039/C0DT01480J.

[52] W. Park, D. Lim, Effect of the oligo(ethylene glycol) group on the antioxidant activity of manganese salen complexes, Bioorg. Med. Chem. Lett. 19 (2009) 614–617, https://doi.org/10.1016/J.BMCL.2008.12.063.

[53] L. Rouco, A. Liberato, M.J. Fernández-Trujillo, A. Máñez, M.G. Basallote, R. Alvariño, A. Alfonso, L.M. Botana, M. Maneiro, Salen-manganese complexes for controlling ROS damage: Neuroprotective effects, antioxidant activity and kinetic studies, J. Inorg. Biochem. 203 (2020), https://doi.org/10.1016/J.JINORGBIO.2019.110918.53.

[54] E.R. Milaeva, D.B. Shpakovsky, Y.A. Gracheva, S.I. Orlova, V.V. Maduar, B. N. Tarasevich, N.N. Meleshonkova, L.G. Dubova, E.F. Shevtsova, Metal complexes with functionalised 2,2′-dipicolylamine ligand containing an antioxidant 2,6-di-tert-butylphenol moiety: synthesis and biological studies, Dalt. Trans. 42 (2013) 6817–6828, https://doi.org/10.1039/C3DT50160D.

[55] H. Wu, C. Wang, F. Wang, H. Peng, H. Zhang, Y. Bai, A New Manganese(III) Complex from Bis(5-methylsalicylaldehyde)-3-oxapentane-1,5-diamine: Synthesis, Characterization, Antioxidant Activity and Luminescence, J. Chinese Chem. Soc. 62 (2015) 1028–1034, https://doi.org/10.1002/JCCS.201500121.

[56] N. Balakrishnan, J. Haribabu, A.K. Dhanabalan, S. Swaminathan, S. Sun, D. F. Dibwe, N. Bhuvanesh, S. Awale, R. Karvembu, Thiosemicarbazone(s)-anchored water soluble mono- and bimetallic Cu(II) complexes: enzyme-like activities, biomolecular interactions, anticancer property and real-time live cytotoxicity, Dalt. Trans. 49 (2020) 9411–9424, https://doi.org/10.1039/D0DT01309A.

[57] B. Kaya, D. Akyüz, T. Karakurt, O. Şahin, A. Koca, B. Ülküseven, Cobalt(II)/(III) complexes bearing a tetradentate thiosemicarbazone: Synthesis, experimental and

theoretical characterization, and electrochemical and antioxidant properties, Appl. Organomet. Chem. 34 (2020) e5930.
[58] Ş. Güveli, Nickel(II)-PPh3 complexes of substituted benzophenone thiosemicarbazones: Electrochemistry, structural analysis, and antioxidant properties, J. Coord. Chem. 73 (2020) 137–153, https://doi.org/10.1080/00958972.2020.1711888.
[59] M. Frisch, G. Trucks, H.B. Schlegel, G. Scuseria, M. Robb, J. Cheeseman, G. Scalmani, V. Barone, B. Mennucci, G. Petersson, Gaussian 09, revision a. 02, gaussian, Inc., Wallingford, CT 200 (2009).
[60] A.D. Becke, Density-functional thermochemistry. III. The role of exact exchange, J. Chem. Phys. 98 (1993) 5648–5652, https://doi.org/10.1063/1.464913.
[61] C. Lee, W. Yang, R.G. Parr, Development of the Colle-Salvetti correlation-energy formula into a functional of the electron density, Phys. Rev. b. Condens. Matter. 37 (1988) 785–789, https://doi.org/10.1103/PHYSREVB.37.785.
[62] Ae. F. James B. Foresman, Exploring Chemistry with Electronic Structure Methods, Exploring Chemistry with Electronic Structure Methods, Gaussian, Inc., Wallingford, CT, 3rd ed., 1996.
[63] R. Dennington, T. Keith, J. Millam, K. Eppinnett, W.L. Hovell, R. Gilliland, GaussView 5.0.8., www.gaussian.com., 2009.
[64] J. He, H. He, M. Cai, F. Zhao, H. He, Insight into the halogen bonding between PA-1 ligand and pyruvate dehydrogenase complex E1 component by crystal structure, DFT calculation, and molecular docking, J. Mol. Struct. 1199 (2020) 126991, https://doi.org/10.1016/J.MOLSTRUC.2019.126991.
[65] M. Malumbres, M. Barbacid, Mammalian cyclin-dependent kinases, Trends Biochem. Sci. 30 (2005) 630–641, https://doi.org/10.1016/J.TIBS.2005.09.005.
[66] M. Hall, G. Peters, Genetic alterations of cyclins, cyclin-dependent kinases, and Cdk inhibitors in human cancer, Adv. Cancer Res. 68 (1996) 67–108, https://doi.org/10.1016/S0065-230X(08)60352-8.
[67] C.J. Sherr, Cancer cell cycles, Science 274 (1996) 1672–1674, https://doi.org/10.1126/SCIENCE.274.5293.1672.
[68] I. Collins, M.D. Garrett, Targeting the cell division cycle in cancer: CDK and cell cycle checkpoint kinase inhibitors, Curr. Opin. Pharmacol. 5 (2005) 366–373, https://doi.org/10.1016/J.COPH.2005.04.009.
[69] G.I. Shapiro, Cyclin-dependent kinase pathways as targets for cancer treatment, J. Clin. Oncol. 24 (2006) 1770–1783, https://doi.org/10.1200/JCO.2005.03.7689.
[70] O. Trott, A.J. Olson, AutoDock Vina: improving the speed and accuracy of docking with a new scoring function, efficient optimization and multithreading, J. Comput. Chem. 31 (2010) 455, https://doi.org/10.1002/JCC.21334.
[71] S. Dallakyan, PyRx-python prescription , in: PyRx-Python Prescr. , The Scripps Research Institute 2010, 2008.
[72] J.A. Maier, C. Martinez, K. Kasavajhala, L. Wickstrom, K.E. Hauser, C. Simmerling, ff14SB: Improving the Accuracy of Protein Side Chain and Backbone Parameters from ff99SB, J. Chem. Theory Comput. 11 (2015) 3696–3713, https://doi.org/10.1021/ACS.JCTC.5B00255.
[73] A. Jakalian, D.B. Jack, C.I. Bayly, Fast, efficient generation of high-quality atomic charges. AM1-BCC model: II. Parameterization and validation, J. Comput. Chem. 23 (2002) 1623–1641. https://doi.org/10.1002/JCC.10128.73 U. Essmann, L. Perera, M. L. Berkowitz, T. Darden, H. Lee and L. G. Pedersen, A smooth particle mesh Ewald method, *J. Chem. Phys.*, 1995, **103**, 8577–8593.
[74] U. Essmann, L. Perera, M.L. Berkowitz, T. Darden, H. Lee, L.G. Pedersen, A smooth particle mesh Ewald method, J. Chem. Phys. 103 (1995) 8577–8593, https://doi.org/10.1063/1.470117.